ELSEVIER

Clinical Neurophysiology 110 (1999) 856–868

Deconvolution of 40 Hz steady-state fields reveals two overlapping source activities of the human auditory cortex

Alexander Gutschalk[a], Ryuzo Mase[a, b], Rainer Roth[a], Nicole Ille[a], André Rupp[a], Stefan Hähnel[c], Terence W. Picton[d], Michael Scherg[a,1]

[a]*Division of Biomagnetism, Department of Neurology, University of Heidelberg, Germany*
[b]*Nihon Kohden Corporation Tokyo, Japan*
[c]*Department of Neuroradiology, University of Heidelberg, Germany*
[d]*Rotman Research Institute, Baycrest Centre for Geriatric Care, University of Toronto, Canada*

Accepted 19 January 1999

Abstract

Steady-state auditory evoked fields were recorded from 15 subjects using a whole head MEG system. Stimuli were 800 ms trains of binaural clicks with constant stimulus onset asynchrony (SOA). Seven different SOA settings (19, 21, 23, 25, 27, 29 and 31 ms) were used to give click rates near 40 Hz.

Transient responses to each click were reconstructed using a new algorithm that deconvoluted the averaged responses to the different trains. Spatio-temporal multiple dipole modelling in relation to 3D MRI scans revealed two overlapping source components in both the left and right auditory cortex. The primary sources in the medial part of Heschl's gyrus exhibited a N19-P30-N40 m pattern. The secondary, weaker sources at more lateral sites on Heschl's gyrus showed a N24-P36-N46 m pattern. When applied to transient middle latency auditory evoked fields (MAEFs) recorded at SOAs of 95-135 ms, the primary sources imaged activities similar to the deconvoluted steady-state responses, but the secondary source activities were inconsistent.

Linear summation of the deconvoluted source waveforms accounted for more than 96% of the steady-state variance. This indicates that the primary activity of the auditory cortex remains constant up to high stimulation rates and is not specifically enhanced around 40 Hz. © 1999 Elsevier Science Ireland Ltd. All rights reserved.

Keywords: Magnetoencephalography; Auditory evoked responses; Temporal processing; Dipole localisation; Auditory cortex

1. Introduction

To process sounds and speech in everyday live, the auditory system must be able to estimate temporal patterns precisely and rapidly. Processing at the level of the auditory cortex can be studied non-invasively with auditory evoked potentials (AEP) or magnetic fields (AEF). However, due to overlap, response waveforms may cancel or enhance each other and form steady-state responses when the interval between the stimuli is shorter than the duration of the response (Regan, 1965, 1982). Galambos et al. (1981) proposed that a periodic 40 Hz auditory event-related potential resulted from the superimposition of successive deflections in the middle latency evoked potential (MAEP). This hypothesis has been supported by synthesis of 40 Hz steady-state response from transient MAEPs and middle latency auditory evoked fields (MAEF) recorded with stimulus rates around 10 Hz (Stapells et al., 1988; Hari et al., 1989; Plourde et al., 1991).

In the first report on auditory MAEPs, Geisler et al. (1958) suggested that they originated in the auditory cortex. Later studies of the scalp topography of the MAEP and of the responses recorded in patients with temporal lobe lesions remained controversial (Vaughan and Ritter, 1970; Picton et al., 1974; Cohen, 1982; Kraus et al., 1982; Wood and Wolpaw, 1982; Woods et al., 1987) although complete abolition of the N_a–P_a component of the MAEP occurred in one patient with bilateral lesions of the auditory cortex (Özdamar et al., 1982).

The predominantly cortical origin of the MAEP has been unambiguously demonstrated by dipole source analysis in patients with lesions, intracranial measurements, and magnetoencephalography (MEG). Scherg and von Cramon (1986) presented a spatio-temporal dipole model to explain

[1] Section of Biomagnetism, Department of Neurology, University of Heidelberg, Im Neuenheimer Feld 400, 69120 Heidelberg, Germany. Tel.: + 49-6221-56-7537; fax: + 49-6221-56-5258.
E-mail address: michael_scherg@med.uni-heidelberg.de (M. Scherg)

1388-2457/99/$ - see front matter © 1999 Elsevier Science Ireland Ltd. All rights reserved. CLINPH 98710
PII: S1388-2457(99)00019-X

the coronal scalp distribution of the MAEP with two dipole sources in each temporal cortex. The response recorded at the vertex showed three main waves: N_a at about 18 ms, P_a at about 30 ms and N_b at about 40 ms, but the response recorded from more lateral electrodes had different peak latencies. The spatio-temporal model separated a primary N9–P30 source component of mainly tangential orientation from a secondary N27–P39 component of more radial orientation. In more than 60 patients with circumscribed vascular temporal lobe lesions affecting either the auditory cortex or the thalamo-cortical auditory radiation, the MAEP source components were reduced or abolished in the lesioned hemisphere, but unaffected in the intact hemisphere (Scherg and von Cramon, 1986, 1990).

Consistent with these findings, human intracranial recordings with depth (Celesia, 1976; Liegeois-Chauvel et al., 1991, 1994) and chronic subdural electrodes (Lee et al., 1984) have demonstrated early cortical responses to auditory stimuli similar to the N19–P30 complex. These responses were recorded from a restricted region on the medial portion of Heschl's gyrus. This area of koniocortex represents the primary auditory cortex (Galaburda and Sanides, 1980).

Confirming results have also been obtained by MEG dipole localisation of middle latency transient (stimulation rates up to 10 Hz) and steady-state fields (periodic stimulation above 10 Hz). Transient MAEFs showed various peaks with consistent source localisation in the superior temporal plane: N19/P30/P50 m (Scherg et al., 1989a; Mäkelä et al., 1994; Yoshiura et al., 1996; Huotilainen et al., 1998) with P30 m as the most prominent peak (Pelizzone et al., 1987; Pantev et al., 1995). Auditory evoked steady-state fields evoked by amplitude modulated (32 Hz) sinusoidal tones with different carrier frequencies showed that the human auditory cortex was tonotopically organised with the lower frequencies more lateral (Romani et al., 1982). Steady-state MAEFs elicited by 40 Hz clicks in trains (Mäkelä and Hari, 1987; Forss et al., 1993) or continuously (Hari et al., 1989) had at least one main source in the superior temporal cortex.

Makeig (1990) reported time-locked MAEP activity in the 40 Hz range in response to clicks presented at slow rates (< 1 Hz). This activity was superimposed on the late N 100 component and separated by using a narrow band-pass filter. The author speculated that clicks presented at these slow rates activated, in addition to the MAEP peaks, one or more oscillatory response generators. MAEFs elicited by a 500 ms toneburst of 1000 Hz and filtered from 28–48 Hz showed a similar oscillatory response named gamma-band response (Pantev et al., 1991; Galambos, 1991). Oscillatory coupling between thalamic and auditory cortex has been suggested to generate both the gamma-band response and the 40 Hz steady-state field (Ribary et al., 1991; Llinas and Ribary, 1991). Galambos (1991) proposed the gamma-band response as the underlying physiological activity for both the transient and the steady state MAEP. Based on single dipole MEG localisations, however, Pantev et al. (1993) suggested that the gamma-band response was generated in a different cortical region from the transient and steady-state MAEF. These transient and steady-state responses were themselves dissociated on the basis of single dipole tonotopical organisation, with the transient MAEFs to lower frequencies being more medial rather than lateral (Pantev et al., 1995, 1996).

The present study separated the 40 Hz steady-state response into its underlying physiological components and identified their related generators in the brain. To achieve this goal, we developed a new algorithm to deconvolute the steady-state responses recorded at several stimulus rates into model transient responses. A paradigm by Mäkelä and Hari (1987) that employed 40 Hz click trains to present trains was modified to use different inter-click intervals (19–31 ms) in the 40 Hz range.

According to previous studies (Hari et al., 1989; Picton et al., 1992), our first hypothesis was that the activity of the primary auditory cortex, as reflected in the N19–P30 complex, should not become either refractory or resonant at stimulation rates between 30 and 60 Hz. In this view the enhanced amplitude at rates near 40 Hz is caused by the superimposition of overlapping transient responses and not by any increased responsiveness at resonant frequencies. We therefore expected that (a) the steady-state response between 30 and 60 Hz can be linearly decomposed into a transient response, and (b) the deconvoluted response is highly similar to the transient response obtained at slow click intervals between 95–135 ms (about 9 Hz).

Based on our previous studies on multiple sources of the MAEP (Scherg and von Cramon, 1986, 1990) and MAEF (Scherg et al., 1989a), we further hypothesised that at least two generating areas in the auditory cortex contribute to the steady-state response. Therefore, spatio-temporal multiple dipole source analysis (Scherg, 1990) was applied to the deconvoluted steady-state responses and source locations were matched with MRI scans.

2. Methods and materials

2.1. Steady-state paradigm

2.1.1. Subjects

Eighteen volunteer subjects without any history of audiological or neurological deficits participated in our study. Informed consent was obtained in all cases. Two subjects had to be excluded from further data analysis due to magnetic or muscular artifacts, and one subject because an MRI could not be obtained. Eight of the remaining 15 subjects were male, 7 female. The mean age was 29 years with a range from 21 to 36 years.

2.1.2. Stimuli

The binaural clicks were generated by passing 0.3 ms

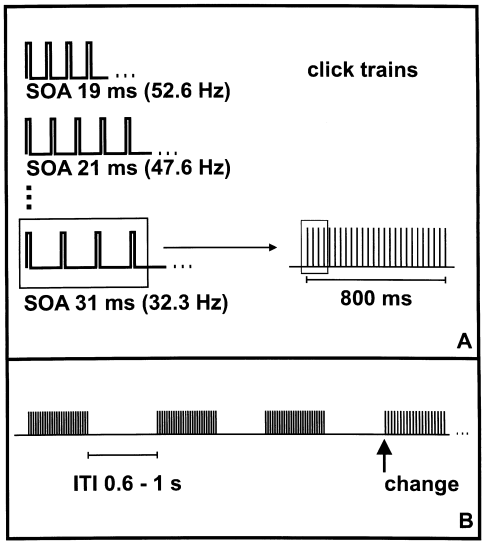

Fig. 1. Steady-state paradigm. A: repetitive clicks of 0.3 ms duration were used to form seven different click trains each lasting 800 ms. The repetition rate or stimulus onset asynchrony (SOA), respectively, was kept constant during the whole click-train at one of 7 settings (19, 21, 23, 25, 27, 29, 31 ms). B: the click trains were presented at inter-train intervals (ITI) randomised between 0.6 and 1.0 s. Trains with a fixed SOA were repeated 4 to 8 times before changing to another SOA setting (cf. Methods).

square waves through special transducers connected to the subject with 50 cm plastic tubes and foam earpieces. Seven different trains were presented at 70 dBnHL (Fig. 1). Each train had a constant repetition rate which varied from 52.6 to 32.3 Hz, i.e. the stimulus onset asynchrony (SOA) between the single clicks in the train ranged from 19 to 31 ms (step-size 2 ms). The 19 ms SOA trains contained 42 clicks, the 21 ms SOA trains 38 clicks etc. so that all trains had a duration of approximately 800 ms.

Click-trains were presented in 4 or 5 runs, each containing 210 trains. The inter-train intervals (ITIs) were randomised from 0.6 to 1.0 s. To minimise stimulus artifacts, click polarity was reversed from one train to the next. Within runs, 30 trains of each SOA were presented. The SOA was changed in alternating up-down steps of 8 or 6 ms using 4 different preset sequences to enable a comparable perception of the virtual pitch change. Each SOA condition was presented 4–8 times before a change occurred.

During recordings, subjects were instructed to keep their eyes open and to fixate a point on the opposite wall. To control attention, subjects were asked to respond to each pitch change by pressing a mouse button.

2.1.3. Procedures and data preprocessing

Recordings were performed in a magnetically shielded room with a Neuromag-122^{TM} whole-head MEG system (Ahonen et al., 1993). At each of 61 sensor positions in the head-shaped arrangement of this system, two figure-of-eight coils with orthogonal orientations measure the planar gradients of the magnetic flux emerging from the head. Prior to MEG recording, 4 position indicator coils were fixed to the subject's head to determine the head position inside the Dewar. For co-registration with MRI, locations of the indicator coils were digitised together with a set of surface points including the nasion and the two pre-auricular points. Head positions were determined at the beginning of each run. MEG data were acquired continuously at a sampling rate of 1000 Hz using a bandpass filter of 0.03–330 Hz. After MEG recordings, a high resolution 3D MRI scan was obtained from all subjects using a Picker Edge MRI scanner (1.5 Tesla).

Data were filtered with a high-pass of 0.3 Hz (12 dB/oct., zero-phase shift Butterworth) and averaged off-line. Noisy channels (0–6, mean 1.7) were excluded from further analysis. To obtain late and sustained evoked fields, the responses to the seven different click-trains were averaged separately over an epoch of 400 ms pre- and 1400 ms post-stimulus onset with artifact-rejection set to exclude about 10% of the sweeps.

Averaged responses were bandpass-filtered from 20 Hz (12 dB/oct.) to 150 Hz (24 dB/oct.) using the zero-phase shift Butterworth filters of the FOCUS program (MEGIS software GmbH, Munich). To obtain steady-state responses, the filtered data were averaged again relative to the single clicks within trains beginning with the fourth click to minimise effects of the response to the train onset. The resulting seven steady-state averaged epochs corresponding to the different inter-click SOAs were baseline corrected and

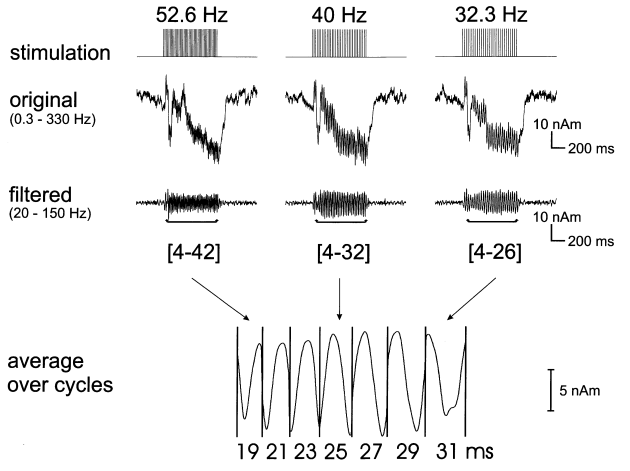

Fig. 2. Steps of data processing prior to deconvolution illustrated for click trains of 52.6 Hz (SOA: 19 ms), 40 Hz (25 ms) and 32.3 Hz (31 ms). The waveforms present the source activity of the right auditory cortex averaged over three recording sessions of subject 1 (400 ms pre-to 1400 ms post-stimulus onset). The source waveforms are obtained by spatial filtering of the 122 averaged MEG sensor waveforms. The wideband waveforms (original) show the prominent P50 m, N100 m and sustained field components overlapped by the 40 Hz activity which is separated by band-pass filtering (filtered). Steady-state fields are obtained by averaging over each cycle starting from the fourth cycle to minimise effects of train onset. Finally, the steady-state fields are concatenated in the order of ascending SOA to form a composite signal of 175 samples (bottom).

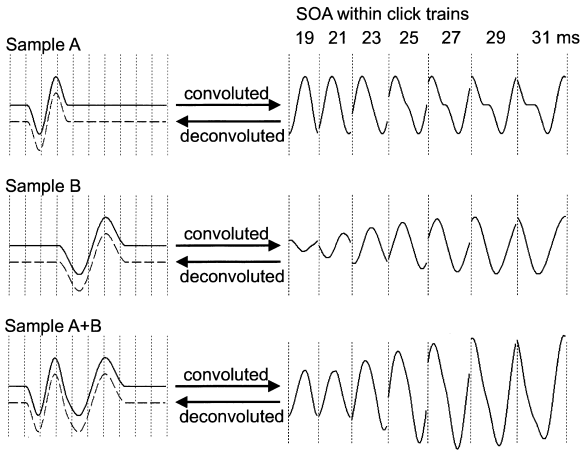

Fig. 3. Simulation testing the linear deconvolution algorithm. Two biphasic waveforms (samples A & B; solid lines, left) and their sum (A + B) are convoluted to a concatenated steady-state response at seven different SOAs (right). Deconvolution of the steady-state response reconstructs the original waveforms identically (dashed lines, left). Amplitude enhancement is seen around 36 Hz for the summed waveform (A + B) after convolution.

concatenated to form a composite waveform of 175 sampling points (Fig. 2).

2.1.4. Temporal deconvolution

The steady-state fields F averaged across all periods at a fixed SOA can be considered to result from the linear overlap of multiple sources in the auditory system (plus noise) on one hand and from the temporal overlap of the transient responses to each click on the other hand. Denoting B as the matrix of the underlying transient model fields and F as the matrix of the steady-state or convoluted fields (row vectors $\boldsymbol{b}_i$ and $\boldsymbol{f}_i$ describe the time signals at each of the 122 MEG sensors) we can write the periodic convolution as a matrix multiplication

$$F = BM \tag{1}$$

with M being the modulation operator which averages the current and preceding single-click responses across the different periodicities. Each column $\boldsymbol{m}_j$ in M will reconstruct one time point in each convoluted response channel $\boldsymbol{f}_i$ when multiplied with $\boldsymbol{b}_i$. Assuming zero amplitude before the click stimulus and after 100 ms, for example, 100 samples (at a sampling rate of 1000 Hz) of the transient response need to be estimated from the steady-state signals. For convenience, the steady-state signal periods were concatenated in an ascending order to form 175 samples (Fig. 2). Thus with a given modulation matrix M the transient model response matrix B can be estimated by applying the pseudoinverse matrix M^{-1} to the right of (1), (I: unit matrix):

$$FM^{-1} = BMM^{-1} = BI = B \tag{2}$$

By reconvoluting the estimated transient response, the residual variance (rv) between the measured and reconvoluted steady-state fields can be calculated in order to test the validity of the hypothesis underlying the modulation matrix M:

$$rv = //F - BM// = //F - FM^{-1}M// = //F\left(I - M^{-1}M\right)// \tag{3}$$

Consistent with previous reports (Hari et al., 1989; Picton et al., 1992), the simplest hypothesis would assume the transient response to be constant within the tested range of

Table 1
Fit ranges and residual variance of linearly deconvoluted source waveforms

	Fit range (ms)				Residual variance (%)	
Subject	Primary source	Secondary source	Primary source	Secondary source	Primary source	Secondary source
	Begin	End	Begin	End		
1	18	21	24	25	0.69	1.32
2	18	21	24	25	2.01	2.46
3	21	24	26	27	1.74	2.72
4	19	22	25	26	1.56	7.49
5	19	22	24	24	0.88	1.05
6	15	19	20	21	4.31	1.3
7	15	19	22	23	-[a]	-
8	18	21	24	25	2.93	6.81
9	17	19	23	24	1.39	1.07
10	17	20	23	24	1.98	1.47
11	18	21	23	24	3.45	2.71
12	20	22	25	26	1.69	4.68
13	16	19	21	22	0.32	-
14	18	21	23	24	3.22	6.35
15	17	19	22	24	1.39	1.26
Median	18	21	23	24	1.72	2.46
Min	15	19	20	21	0.32	1.05
Max	21	24	26	27	4.31	7.49

[a] No stable bilateral dipole model found.

steady-state SOAs (19–31 ms). For an SOA of 19 ms, for example, the first column vector $\boldsymbol{m}_1$ in M has zero-valued elements except for the 1st, 20th, 39th, etc. elements having values of 1. Likewise the second time point in $\boldsymbol{f}_i$ is constructed by convolution with $\boldsymbol{m}_2$ having non-zero 2nd, 21st 40th etc. elements of value 1. After the 19 vectors for the fastest cycle (52 Hz), $\boldsymbol{m}_{20}$ will begin again with a non-zero 1st followed by non-zero 22nd, 43rd etc. elements having a spacing corresponding to the 21 ms cycle, and so on. As an example, imagine a modulation operator for concatenated data in ascending order with SOAs of 4, 5, and 6 ms and a sampling rate of 1 ms to convolute a 12 ms response:

4 ms				5 ms cycle					6 ms cycle					
1	0	0	0	1	0	0	0	0	1	0	0	0	0	0
0	1	0	0	0	1	0	0	0	0	1	0	0	0	0
0	0	1	0	0	0	1	0	0	0	0	1	0	0	0
0	0	0	1	0	0	0	1	0	0	0	0	1	0	0
1	0	0	0	0	0	0	0	1	0	0	0	0	1	0
0	1	0	0	1	0	0	0	0	0	0	0	0	0	1
0	0	1	0	0	1	0	0	0	1	0	0	0	0	0
0	0	0	1	0	0	1	0	0	0	1	0	0	0	0
1	0	0	0	0	0	0	1	0	0	0	1	0	0	0
0	1	0	0	0	0	0	0	1	0	0	0	1	0	0
0	0	1	0	1	0	0	0	0	0	0	0	0	1	0
0	0	0	1	0	1	0	0	0	0	0	0	0	0	1

In summary, the hypothetical BM matrix multiplication would calculate a value at each time point in each channel equal to the sum of the evoked responses to each of the preceding clicks within the period of time that they might still be active, and concatenates the responses according to the different SOAs. The actual FM^{-1} multiplication will then derive the single-click evoked response from the concatenated responses that were recorded.(Fig. 3)

Non-linear hypothesis testing can be achieved by attenuating non-zero values for shorter SOAs and later latencies. SOA- dependent and latency-dependent non-linear delays of the evoked response can be introduced by advancing and distributing later non-zero values within a column to previous rows. Thus, non-linear amplitude decreases and latency delays of later response components can be modelled using this approach. However, the linear hypothesis resulted in extremely low residual variances in all subjects (Table 1) which did not leave sufficient variance to model a potential non-linear effect. In addition, if the response did change with SOA, the model should have fit some SOA responses better than others. However, *rv* did not change systematically across steady-state frequencies. Therefore, we did not further investigate non-linear hypotheses after initial tests which did not yield a consistent improvement in residual variance.

In order to analyse our concatenated steady-state fields, a non-zero transient model response pattern of 130 samples following the click stimulus was reconstructed assuming zero response activity after 130 ms. The pseudoinverse matrix M^{-1} was calculated using SVD (Press et al., 1992) and retaining 99% of the variance in the eigenvalues to obtain a stabilising regularisation. Implicitly, the selected range of periodicities results in a high-pass filtering of the underlying transient evoked response by the inverse operator M^{-1} with a 6 dB cut-off at 32 Hz. Hence, transient and steady-state data were filtered with a high-pass filter at 20 Hz as described above to facilitate comparisons and to avoid excessive noise due to low frequency activity.

2.1.5. Multiple source analysis and temporal deconvolution

Using the spatio-temporal multiple source model (Scherg and von Cramon, 1985; Scherg and von Cramon, 1986; Scherg, 1990), the evoked magnetic fields B can be described by the linear overlap of discrete source activity waveforms $\boldsymbol{s}_k$ to be combined in matrix S [n of sources (samples]

$$B = CS \tag{4}$$

The fixed location and orientation of the N equivalent dipole sources exhibit stationary field distributions (topographies) $\boldsymbol{c}_k$ which are described by columns in the forward solution matrix C. Similar to the temporal deconvolution in (2), the source activities S can be estimated by a spatial deconvolution (or spatial filter) defined by the pseudoinverse of C:

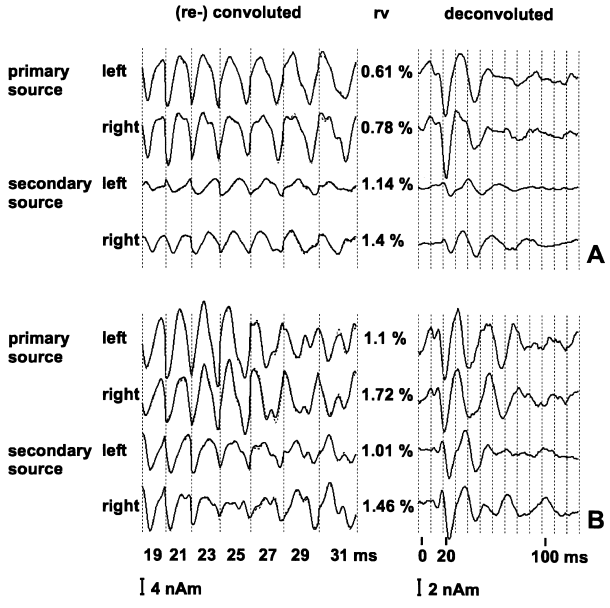

Fig. 4. Source waveforms of recorded steady-state signals (= convoluted, solid lines, left) and the corresponding deconvoluted responses (right) of two subjects (A, 1; B, 15). Reconvoluted responses as computed from the deconvoluted waveforms are plotted on top (dotted lines, left) for comparison. Differences between the recorded and reconvoluted data are very small for all SOAs (cf. *rv*: residual variances, middle). Resonance enhancement is not observed. Apparent maxima in the steady-state responses vary between subjects according to the underlying transient waveshape (A, 29 ms period; B, 23 ms period). Note the different amplitude scaling of steady-state and deconvoluted source waveforms.

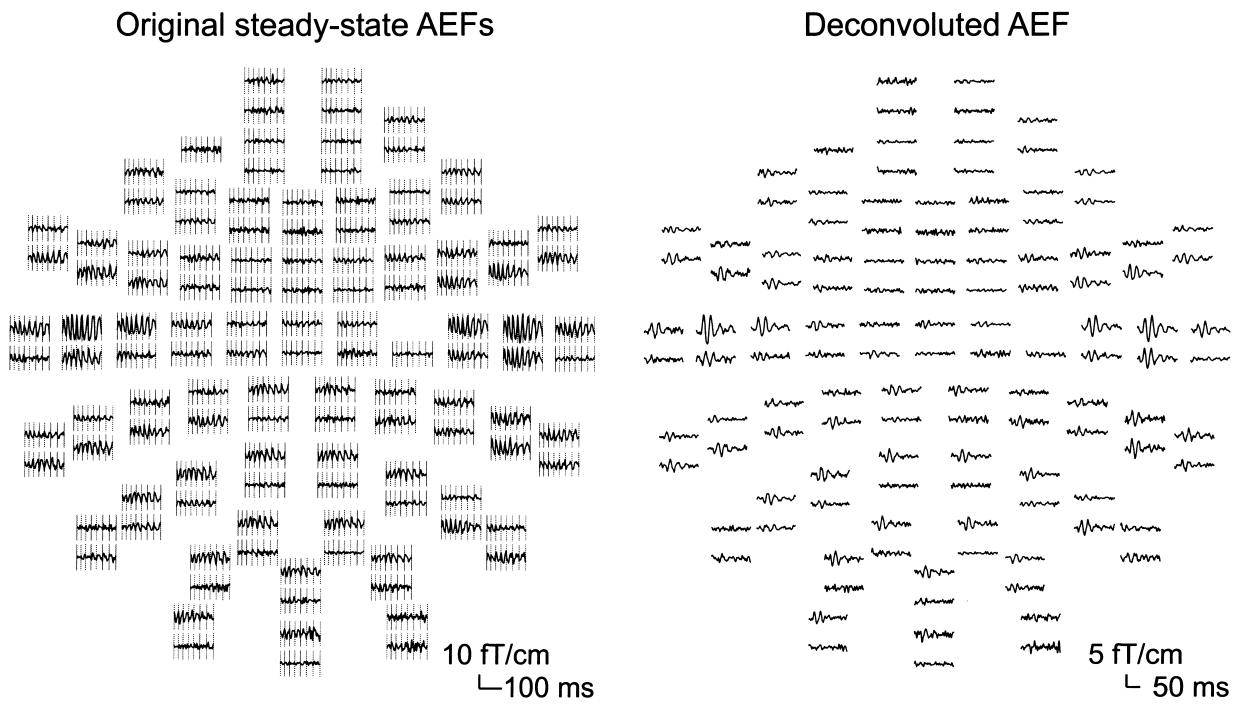

Fig. 5. Original steady-state (left) and deconvoluted (right) MEG data set of subject 9. The 122 planar gradiometer signals of the Neuromag-122™ system are displayed in top view with the latitudinal and longitudinal derivatives of each sensor plotted in pairs above each other. Two bad channels have been switched off. Focal auditory evoked activity is seen over both temporal lobes. Due to the origin of the signals deep inside the Sylvian fissure maximum peak-to-peak gradients are only in the order of 10fT/cm in the deconvoluted data.

$$S = C^{-1}B \tag{5}$$

Applying (4) to (1) and operating with the spatial filter from the left and with the temporal deconvolution from the right, we get an estimate of the transient source activity matrix S

$$C^{-1}FM^{-1} = C^{-1}CSMM^{-1} = SMM^{-1} = SI = S \tag{6}$$

Since both operations are linear, we were able to deconvolute in time and localise sources interactively (Scherg, 1990) using the BESA® program (MEGIS Software GmbH Munich). Alternatively, we could first obtain the convoluted source activities using the spatial source filter and thus assess the residual variance of the temporal deconvolution model (Fig. 4).

Mapping of the field distribution normal to the level of the MEG whole head sensor array was done by employing the minimum norm estimate using the Neuromag-122™ software. For MEG source analysis, a spherical head model was used (Hämäläinen and Sarvas, 1987). The origin of the sphere was estimated for each subject from individual MRI scans (Ahonen et al., 1993). Using the head position indicators, dipole positions were mapped onto the individual MRI scans to study the anatomical relevance and plausibility of solutions using the Neuromag-122™ software. Peak latencies and amplitudes of source waveforms were measured using the BESA® program. Further details about the source analysis are described along with the respective data sets in the results section.

2.1.6. Transient paradigm

To compare the results of deconvolution with transient MAEFs, 5 subjects (2 female, mean age 29) were studied in a second experiment. Three subjects were measured in the same recording session in which steady-state responses were obtained, and two subjects were studied in separate sessions.

Clicks (0.3 ms duration) were presented binaurally at pseudo-randomised SOAs ranging from 95 to 135 ms. Single click intensity was kept identical to the steady-state experiment. Stimuli were grouped in 4 or 5 sets of 4000 clicks each, and recordings were performed in the same way as described above.

Averages were computed off-line with a 0.3 Hz highpass filter applied to the raw data. Bad channels were excluded and artifact rejection was used to omit about 10% of the sweeps. Averaged data was bandpass filtered between 20 (12 dB/oct.) and 150 Hz (24 dB/oct.) with a zero-phase shift Butterworth filter applied to a segment from 100 ms before to 200 ms after the stimulus. The same 130 ms interval post-stimulus was segmented for comparison with the deconvoluted data.

3. Results

3.1. Steady-state paradigm

3.1.1. Deconvoluted MEG data and field maps

Deconvolution of the steady-state MEG signals resulted

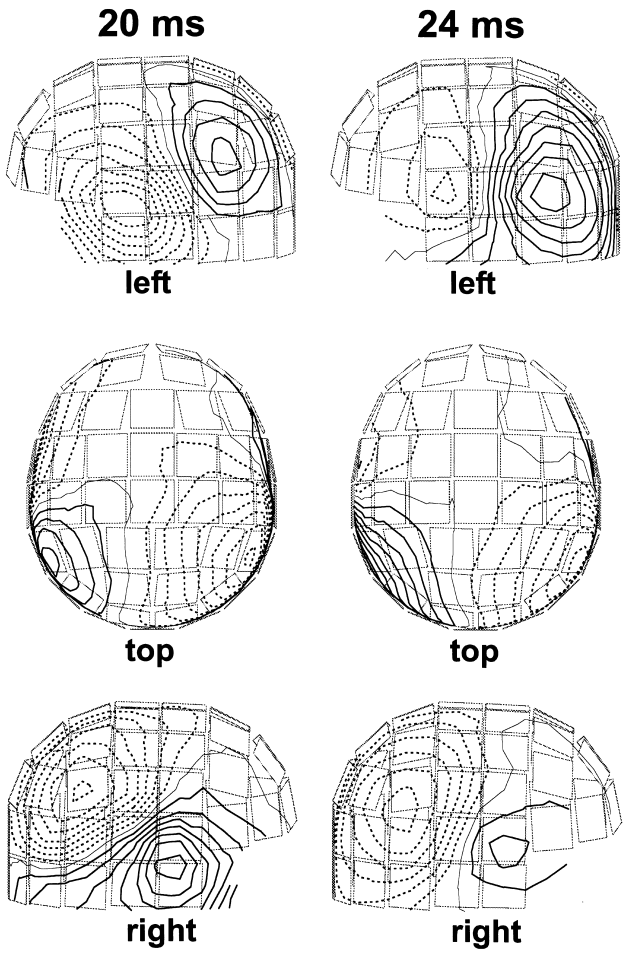

Fig. 6. MEG field maps of the deconvoluted signals of subject 9 at 20 ms and 24 ms (contour step 2 fT). The change in orientation of the bilateral dipolar pattern between these latencies suggests the contribution of at least two sources in each temporal lobe.

in a transient-like activation pattern in all subjects. In the planar gradiometers, the deconvoluted steady-state response showed a symmetric distribution with maximum amplitudes over both temporal lobes (Fig. 5). Waves N_am, P_am, N_bm and P_bm were consistently observed over the Sylvian fissures bilaterally. At different sensors, peak latencies varied from 17–23, 27–33, 39–45 and 51–56 ms for components N_am to P_bm. Occasionally, N_am was preceded by a small earlier deflection in the range of 8–15 ms. In two subjects repeated measurements over 2–3 days showed excellent response reproducibility.

Mapping of the field distribution of waves N_am to P_am showed dipolar activity over both temporal lobes. In the latency range from N_am onset to P_am, the field patterns remained dipolar over the Sylvian fissure, but the orientation of the dipolar field pattern changed. The oblique forward orientation on the rising edge of N_am commonly turned more towards vertical during the falling edge of N_am and back during P_am (Fig. 6). This sequence could be seen in 11 of the 15 subjects. In subjects 6, 8 and 15, the dipolar pattern turned from a vertical orientation forward. Subject 7 exhibited the common dipolar field rotation pattern over the right hemisphere, but showed a dipolar pattern at more parietal sites over the left hemisphere. This subject's MRI showed an unusual anatomical orientation of the medial part of the left Heschl's gyrus.

3.1.2. Steady-state field sources in the auditory cortex

The rotation pattern suggested at least two generators in each hemisphere with temporally overlapping activities to contribute to the N_am–P_bm complex (Scherg, 1990). To estimate equivalent sources, two short epochs in the time range of the N_am deflection were chosen at which the field topography remained stable. The first epoch was selected from the onset of N_am to the peak and the second at the end of N_am (Table 1). At each of these intervals, a bilateral dipole pair was fitted simultaneously. Fitting was started from a symmetrical configuration with one dipole in each temporal lobe. The fit of a third dipole pair in the latency of N_bm to P_bm resulted in strong interactions between all dipoles, indicating that the separation and imaging of 3 source activity patterns in each hemisphere was impossible. Finally, the 4 dipole configuration as fitted to the earlier intervals was used as a spatial filter to image two different activation patterns of each temporal lobe over the whole response epoch and to examine their consistency across subjects.

In the first interval around 19 ms, the dipole fit resulted in a configuration of a bilateral dipole pair in all cases except subject 7. Projection into the MRI-scan revealed a position at the medial aspect of Heschl's gyrus in 25 out of 28 hemispheres. Both dipole positions in subject 2 and the right in subject 6 were located about 4–6 mm above the medial portion of the Sylvian fissure. In the second interval around 24 ms, a separate dipole pair could be fitted in 13 out of 15 cases. In subject 13, a dipole could only be fitted in the right hemisphere. All 27 dipoles fitted in the second interval were located lateral to those obtained in the early interval. In an ANOVA for repeated measurements, the difference between the 3D locations of the primary and secondary sources was significant for both hemispheres (right: $df = 2.12$ $F = 24.79$ $P < 0.001$; left: $df = 2.11$ $F = 5.65$ $P < 0.05$). Secondary dipoles were located at Heschl's gyrus or planum temporale in 23 out of 27 hemispheres. In 3 hemispheres, dipoles were located above the Sylvian fissure and in one at the white matter below Heschl's gyrus. This was probably due to MEG source localisation inaccuracy and overlap in the second interval. Thus, the constellation with primary dipoles at medial Heschl's gyrus and secondary dipoles lateral from primary dipoles at Heschl's gyrus or planum temporale was observed in 20 hemispheres, not considering the cases with locations above the Sylvian fissure or in white matter. The median distance between the medial and lateral dipoles was 11.4 (8.2 − 16.7) mm for right ($n = 10$) and 11.3 (5.0 − 32.2) mm for left hemispheres ($n = 10$). Fig. 7 shows a representative example of dipole localisations co-registered with MRI.

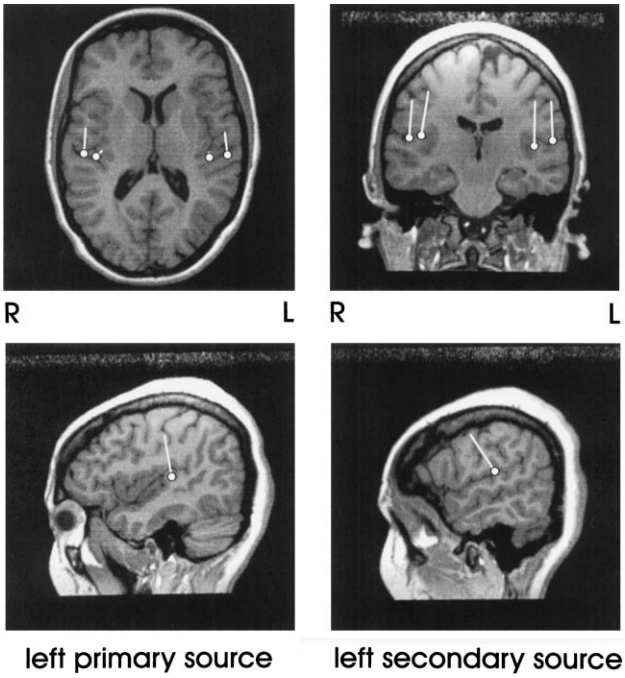

Fig. 7. Dipole sources of subject 15 co-registered with MRI in axial, coronal and sagital views. The primary sources (N19 –P30 m) are located at the medial aspect of Heschl's Gyrus deep inside the Sylvian fissure. The secondary sources are located about 1 cm more laterally.

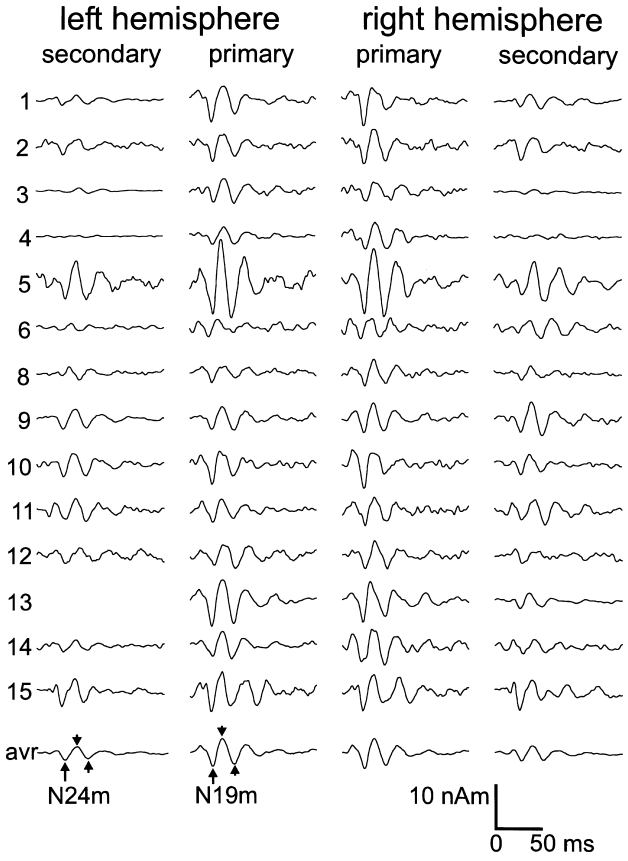

Fig. 8. Deconvoluted dipole source waveforms of all subjects except subject 7 (cf. text). Grand average source waveforms are shown at the bottom (avr). Primary peaks N19, P30 and N41 m and secondary peak N24, P36 and N46 m (arrows) are consistently observed. Current magnitudes of the primary sources were about twice those of the secondary sources. In subjects 3 & 4, the secondary dipoles estimated only a small superficial source current (2,3). In subject 13, the left secondary dipole fit was unstable.

Fig. 8 depicts the source waveforms of all subjects except subject 7. The medial and lateral source activities exhibited similar waveforms with the lateral activities delayed by 5–7 ms. The primary, medial source activity peaked at N19, P30 and N41 m, the lateral at N24, P36 and N46 m. In subjects 3 and 4, the lateral sources were very superficial and showed only a weak activity pattern. Primary source currents were about twice the size of the secondary currents (Table 2).

3.1.3. Accuracy of temporal deconvolution

The accuracy of the deconvolution procedure was tested by reconvoluting the steady-state responses from the 4 source waveforms derived in each subject and then comparing the reconvoluted and original source waveforms obtained by applying the spatial source filter to the concatenated steady-state responses (Fig. 4). Reconvoluted steady-state waveforms accounted for 98.3% (median, range: 95.7–99.3%) of the original primary and for 97.5% (median, range: 92.5–99.0%) of the original secondary source waveforms. Calculated for all source waveforms together, they accounted for 98.2% (median, range: 96.2–99.6%) of the variance. Residual variances between original and reconvoluted source waveforms are listed in Table 1.

3.1.4. Evolution of the steady-state fields during click trains

To investigate the stability of the source components during the click trains, we compared 4 subaverages over different epochs during the train comprising: (a) click responses 1–8, (b) 20–N (N = 42 to 26 depending on periodicity), (c) 4–N (data presented above; Fig. 8). The primary component was highly similar in all subaverages in amplitude. Only the secondary component showed a non-significant increase in amplitude towards later clicks in the train. Mean latencies of the later 20–N steady-state epoch were prolonged relative to the early subaverage 1–8. This increase was 1.2, 3.2 and 3.3 ms for the primary N19/P30/N41 m peaks, respectively, and 0.4, 2.8 and 3.5 ms for the secondary N24/P36/N46 m peaks. It was significant for all component waveforms except for the left secondary component (ANOVA for repeated measurement, $P < 0.05$). The differences between the average waveforms used for the analysis (4-N) and the later average (20–N) were negligible in both amplitude and latency except for a small increase in peak latencies of the later 20–N average (range 0.3–1.9 ms, significant at $P < 0.05$ only for the left primary source component).

3.1.5. Transient paradigm

3.1.5.1. MAEF surface data Using single click stimuli at ISIs of 95–135 ms, MAEF response peaks N_am, P_am, N_bm and P_bm could be identified consistently in all 5 subjects. The distribution was symmetrical with maximum planar gradiometer amplitudes and dipolar field patterns over both temporal lobes.

3.1.5.2. MAEF source imaging Source imaging of the transient MAEFs with the dipole model obtained from the deconvoluted data showed source waveforms similar to the primary transient sources. Source activity peaks N19 and P30 m were observed in all subjects. In the transient primary source waveforms, the deflection around 41 ms (N41 m) was more variable than the same peak in the deconvoluted data, possibly due to the larger noise level of the transient MAEF. The transient MAEF showed a slightly earlier N19 m and later P30 m as compared to the deconvoluted steady-state peaks (Table 2). However, this difference was not significant. The secondary sources imaged no consistent activation pattern following transient single click stimulation. Source waveforms to both stimulations are overlayed in Fig. 9 for comparison.

4. Discussion

4.1. Sources for the MAEF in the auditory cortex

Spatio-temporal source analysis of the deconvoluted response indicated that two cortical sources with temporally overlapping activation patterns contribute to the auditory steady-state field. A primary source with an N19–P30–N41 m activity could be separated from a secondary source with an N24–P36–N46 m pattern. This could explain why Hari et al. (1989) found that the localisation of a single dipole model of the 40 Hz steady-state field changed systematically by about 1 cm with a period of 7–8 ms. Similar observations have been reported by Pantev et al. (1996) on steady-state fields evoked by repeated Gaussian tone pulses. Temporally overlapping sources in different areas of auditory cortex have also been reported for the late human AEPs (Scherg and von Cramon, 1985; Scherg et al., 1989b) and the auditory middle latency response of rats (Barth and Di, 1991). Ribary et al. (1991) suggested thalamic and cortical sources for the 40 Hz steady-state field with the thalamus scanning widespread regions of the cortex. We cannot rule out an additional subcortical source, but the different field orientations and the more lateral source localisations around 24 ms are clear evidence that multiple focal generators in the auditory cortex are the predominant source of the 40 Hz auditory steady-state field.

The localisation of our first source to the medial part of Heschl's gyrus and the 19.4 and 29.1 ms peak latencies of the corresponding source waveforms suggest that the activity is generated in the primary auditory cortex. This is supported by intracranial recordings (Celesia, 1976; Lee et al., 1984; Liegeois-Chauvel et al., 1991, 1994). The high similarity of the deconvoluted and transient MAEFs suggests that they represent the same cortical process.

The nature of our second source remains unclear. Four different hypotheses can be considered:

1. The secondary component might be specific for steady-state or rapid stimulation. It could represent the temporal processing of repetitive events. In order to perceive the different pitches of the click-trains the cortex would have to monitor the intervals between the clicks. This hypoth-

Table 2
Latencies and amplitudes of peaks in source waveforms

		Mean latency ± SD (ms)		Mean amplitudes (range) (nAm)		Number of subjects[a] *n*	
		Deconvoluted	Transient	Deconvoluted	Transient	Deconvoluted	Transient
Primary component							
N19	Right	19.4 ± 1.7	18.4 ± 0.6	4.1(2.4–7.4)	4.8(2.6–7.4)	14	5
	Left	19.5 ± 1.4	18.8 ± 1.0	3.6(1.9–7.3)	4.0(1.9–7.5)	14	5
P30	Right	28.8 ± 1.4	30.7 ± 1.4	3.5(2.0–7.7)	3.9(2.5–6.0)	14	5
	Left	29.4 ± 1.9	31.3 ± 1.5	3.3(1.1–9.8)	5.0(3.0–7.9)	14	5
N41	Right	40.6 ± 1.9	43.5 ± 2.1	3.2(1.4–7.9)	3.0(1.0–5.1)	14	5
	Left	41.1 ± 1.7	42.4 ± 1.7	3.1(1.2–8.5)	3.4(2.1–5.1)	14	5
Secondary component (m)							
N24	Right	23.8 ± 1.3	-	2.2(1.1–4.1)	-	12	-
	Left	24.0 ± 1.7	-	2.0(0.6-3.9)	-	11	-
P36	Right	35.2 ± 2.2	-	2.3(0.7–4.8)	-	12	-
	Left	36.0 ± 3.2	-	2.1(0.9–4.8)	-	11	-
N46	Right	46.2 ± 2.7	-	2.1(0.8–4.2)	-	12	-
	Left	46.1 ± 3.9	-	1.8(0.7–4.0)	-	11	-

[a] Components with baseline to peak source current < 0.5 nAm excluded.

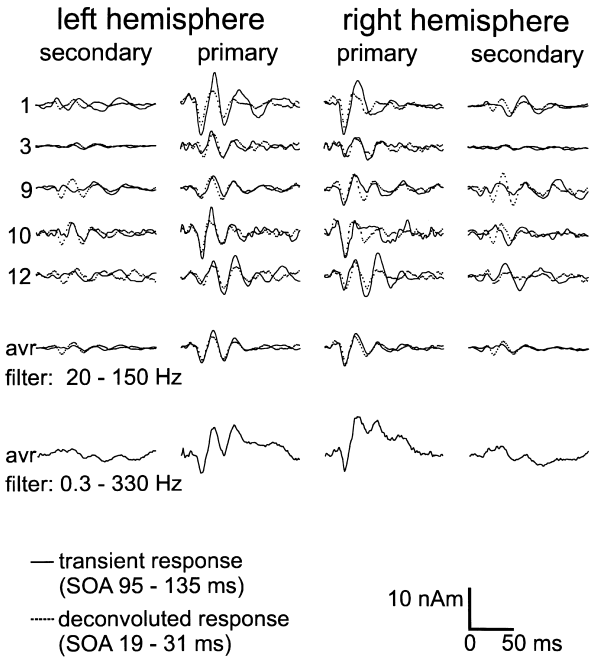

Fig. 9. Comparison of transient (solid lines) with deconvoluted (dotted) source waveforms in 5 subjects. Grand mean displayed at the bottom (avr). The 4-dipole model was fitted to the deconvoluted data and then used as a spatial filter to decompose the transient data into source waveforms for comparison. The primary N19–P30 m source component is similarly observed for both types of stimulation. As in MAEPs, it is the most prominent component of the broad-band (0.3–330 Hz) transient response. Deflections following P30 m are more variable in the transient as compared to the deconvoluted responses. Transient secondary source activities are quite variable across subjects while the deconvoluted secondary source waveforms depict a consistent N24–P36–N46 m pattern.

esis could account for the inconsistent waveforms recorded for the transient MAEFs where such temporal processing is unnecessary.

2. The second source might represent the tangential projection of a predominantly radial current source. Scherg and von Cramon (1986) described two overlapping sources for the MAEP. In addition to a tangential dipole modelling the N19–P30 component they found a radial dipolar source active 8 ms later. Since radial components remain undetected in the MEG, only a weak tangential projection of this mainly radial component would be expected in magnetic recordings. This limitation as well as the fact that the secondary component reported here was not found in the transient data argue against this hypothesis. A more detailed comparison between deconvoluted and transient responses, using both electrical and magnetic recordings would be needed to assess this hypothesis.
3. It is possible that the secondary component might depend on the subject paying attention to the stimuli, or to some particular aspect of the stimuli. The auditory regions of the primate cortex appear to be organised into a central core area, surrounded by belt and parabelt regions (Morel and Kaas, 1992). The core regions are probably automatically activated by incoming auditory information, but the belt and parabelt regions may only be activated if the connectivity is facilitated by some attentional processing (Olshausen et al., 1993; Grady et al., 1997).
4. The source might represent a response to low-frequency stimuli. Clicks have a wide frequency spectrum. Stimulation at lower frequencies elicits responses with longer latencies than stimulation at higher frequencies (Scherg and Volk, 1983; Scherg et al., 1989a). Our second dipole might therefore model the processing of low frequencies in more lateral sites of primary auditory cortex. A weak point in this hypothesis is that it cannot explain why we did not find the same activity in transient responses.

4.2. Source activation patterns and scalp-recorded peaks

Temporal integration of successive stimuli could require prolonged activation in the involved generators. One characteristic finding in our deconvoluted data is the constancy of wave N_bm (respective N41 and N46m in source waveforms) which has been reported to be rather inconsistent between subjects (e.g. Özdamar and Kraus, 1983). A similar effect has been reported by Picton et al. (1992) who found N_b being more pronounced to stimulation at ISIs of 13–37 ms than at longer ISIs using maximum length sequences. They ascribed this effect to an additional generator in the range from 30 to 50 ms with a steeper recovery function than N_b (see also Erwin and Buchwald, 1986a). Part of the inconstancy regarding N_bm may, therefore, depend on the different amounts of highpass filtering which attenuates the overlapping P50 component and thereby enhances N_bm. On the other hand, MAEPs recorded during natural slow-wave sleep have shown disappearance of wave N_b while N_a and P_a could still be recorded (Erwin and Buchwald, 1986b; Deiber et al., 1989).

From intracranial recordings, a triphasic response pattern with peaks at 14, 19 and 30 ms is concordantly assumed as the response of the primary auditory cortex. (Celesia, 1976; Lee et al., 1984; Liegeois-Chauvel et al., 1991). Later deflections recorded from the same site as the early cortical response were only reported inconsistently (Celesia, 1976; Liegeois-Chauvel et al., 1994) or could not be observed because the averaged epoch was too short (Lee et al., 1984; Liegeois-Chauvel et al., 1991). A distinct generator has been described for the P50 component in a more lateral part of primary auditory cortex by intracranial recordings (Liegeois-Chauvel et al., 1994) and has similarly been reported from MEG data (Scherg et al., 1989a). While N19 and P30 m were found to mirror the primary auditory cortex response, the nature of N41 m can not be derived from the available intracranial data. Our source analysis suggests that N41 m is an additional deflection of the primary auditory cortex response and contributes to N_bm together with N46 m of our secondary source. Whether the consistency of N41 and N46 m we observed is caused by processing specific to the periodic stimuli we used cannot as yet be definitely answered.

4.3. Transient and steady-state responses

The present results support the hypothesis that the 40 Hz steady-state response mainly represents the overlapping of transient waveforms. Low residual variance between recorded and reconvoluted signals indicates that a linear model works well for the range of SOAs chosen in the present experiment. Individual waveform patterns of the transient response can account for the amplitude enhancement at rates near 40 Hz without recourse to further explanation. This is consistent with the findings of Picton et al. (1992) who reported latencies and amplitudes of N_a, P_a and N_b to remain stable at ISIs from 13 to 37 ms. It has also been shown before that the auditory steady-state responses can be reconstructed from transient middle latency responses (Stapells et al., 1988; Hari et al., 1989; Plourde et al., 1991). In this study click trains of 800 ms duration instead of a continuous steady-state paradigm have been used for the evaluation of the deconvolution technique. However, the observed fast stabilisation of the response during the train, in particular in amplitude and waveshape, suggests that our results also apply to continuous steady-state responses.

We did not find any clear effect of increasing stimulus rate on the response. This would have disrupted the deconvolution procedure unless additional parameters were included. Our results therefore differ from those of Azzena et al. (1995), who found that the steady-state electrical response at 60 Hz was smaller than that synthesised by adding together transient responses. They found the opposite effect at 30 Hz although this did not appear to reach significance. They interpreted these effects as indicating that the response decreases in amplitude and increases in latency with increasing rate. Their rates were slightly beyond those studied in our experiment (32.2–52.6). However, our data did not provide any suggestion of rate-dependant effects. Another possible explanation for the differences is that they recorded a much smaller number of responses (2000). The response may be more stable both physiologically and technically (less residual noise) when the recordings are based on many more responses.

Santarelli et al., (1995) have suggested that the electrical auditory steady-state response at 40 Hz contains activity related to some resonant activity in the auditory system in addition to the superimposed transient responses. Their main evidence was that the response to the last click in a train of clicks contained activity that was different from the response to a single click or to the average response to the clicks within the train. However, we consider it more likely that the auditory system generated an offset-response at the end of the train.

The deconvoluted responses resemble the response pattern that is commonly known for MAEFs. Latency ranges of N_am, P_am, N_bm and P_bm were found to be congruent with those that have been reported for transient MAEFs and MAEPs. Activity in the 40 Hz range at latencies up to 130 ms reported to be characteristic for the transient gamma-band response was not observed in our data. This supports the hypothesis that the gamma-band response is different from the processes responsible for auditory middle latency and steady-state responses and can only be recorded at slow stimulation rates (Makeig, 1990; Pantev et al., 1993).

Franowicz and Barth (1995) showed that the 40 Hz response in the auditory cortex of the rat is quite distinct from spontaneous gamma-band activity which fluctuated in its spatio-temporal distribution. They also found that the steady-state response generated in the auditory cortex involved a more focal region of the cortex than the normal transient response. This suggests that the steady-state response may be generated by only a subset of the neurons that respond to transients. Our results do not fit easily with these findings. The fact that the rats were lightly anaesthetised might have limited the extent of the steady state response more than the transient response. It is also possible that focal sources and more widely distributed sources may have similar effects at some distance from the cortex. Although we cannot rule out this possibility, we consider the anaesthesia explanation more likely.

Pantev et al., (1995, 1996) found different tonotopic organisations for P_am and steady-state fields. They assumed that a steady-state field composed of successive MAEFs should mainly consist of wave P_am. Using a single dipole analysis, they concluded that the steady-state field was generated differently from the transient MAEF (Pantev et al., 1995). As shown here, however, the steady-state field is composed of waves N_am, P_am, N_bm and P_bm in an equivalent relation with at least two contributing sources. It is possible that an analysis using two sources and a more complex source waveform might make the tonotopic organisations of the transient and steady-state MAEFs more homologous, but this hypothesis will need experimental evaluation. The question is complex since different regions of the auditory cortex have mirror-symmetric tonotopic organisations (Morel et al., 1993; Rauschecker et al., 1995, 1997; Kosaki et al., 1997).

4.4. Analysis techniques for steady-state responses

This paper shows that deconvolution improves the analysis of auditory steady-state responses. Conventional analysis of steady-state responses is restricted by filter effects of the averaging procedure and the temporal convolution of components. The ‘apparent latency’ which can be calculated by linear regression of the phase delay at different rates of stimulation has been used to further characterise steady-state responses (Regan, 1982; Picton, 1987). Yet, Hari et al. (1989) have shown that this is only a nonspecific estimate and cannot be used to describe the latency of a convoluted response.

Deconvolution allows to study the particular waveforms which overlap to the periodic response recorded at steady-state stimulation. The technique requires stimulation at

different frequencies and, therefore, the linear approach can only be successful if the overlapping response remains stable over the used range of stimulation frequencies.

MAEPs at ISI ranges comparable to our present study have been reported before by Picton et al., (1992) using maximum length sequences (MLS). An MLS can be used to control the order of sensory stimuli in a way that allows to remove the overlapping responses at fast stimulation. This technique was first used by Eyshold and Schneider (1982) to record auditory brainstem responses. Drawbacks of this method are the wide ISI range employed in averaging which is assumed to elicit the same response and the dependency of stimulation on a fixed sequence.

A so-called 'Adjar' technique to remove overlapping responses has been proposed by Woldorff and Hillyard (Woldorf and Hillyard, 1991; Woldorff, 1993). Based on the conventional average and the known ISI jitter the effect of overlapping is estimated and subtracted. This method can be applied once or in an iterative algorithm. While this method is flexible in not restricting the design of paradigms, it depends, on the other hand, on an initial average to estimate the effects of overlapping.

The deconvolution technique introduced in this report might be another interesting tool in further investigations on early cortical processing. Used with frequency-specific stimuli and electrically obtained data (in addition to the magnetic data), it could help further our knowledge of the physiology of the human auditory cortex. Major questions concern the representation of pitch, spectral and temporal cues in the primary and secondary areas of the auditory cortex. Using a non-linear approach for deconvolution should allow one to look at possible refractory effects of rapid stimulation. These effects did not show up in our results but might be important in data obtained at different stimulation rates and in other modalities.

Acknowledgements

We wish to thank Martina Kirsch and Esther Tauberschmidt for their help on recording and stimulus generation. We gratefully acknowledge industrial grand support from Picker International GmbH, Germany, from Nihon Kohden Corporation, Japan, and from MEGIS Software GmbH, Germany.

References

Ahonen AI, Hämäläinen MS, Kajola MJ, Knuutila JET, Laine PP, Lounasmaa OV, Parkkonen LT, Simola JT, Tesche CD. 122-Channel SQUID instrument for investigating the magnetic signals from the human brain. Physica Scripta 1993;T49:198–205.

Azzena GB, Conti G, Santarelli R, Ottaviani F, Paludetti G, Maurizi M. Generation of human auditory steady-state responses (SSRs) I. Stimulus rate effects. Hearing Res 1995;83:1–8.

Celesia GG. Organization of auditory cortical areas in man. Brain 1976;99:403–414.

Cohen MM. Coronal topography of the middle latency auditory evoked potentials (MLAEPs) in man. Electroenceph clin Neurophysiol 1982;53:231–236.

Barth DS, Di S. The functional anatomy of middle latency auditory evoked potentials. Brain Res 1991;565:109–115.

Deiber MP, Ibanez V, Bastuji H, Fischer C, Mauguiere F. Changes of middle latency auditory evoked potentials during natural sleep in humans. Neurology 1989;39:806–813.

Erwin RJ, Buchwald JS. Midlatency auditory evoked responses: differential recovery cycle characteristics. Electroenceph clin Neurophysiol 1986;64:417–423.

Erwin RJ, Buchwald JS. Midlatency auditory evoked response: differential effects of sleep in the human. Electroenceph clin Neurophysiol 1986;65:383–392.

Eyshold U, Schneider C. Maximum length sequences - a fast method for measuring brainstem evoked responses. Audiology 1982;21:242–250.

Forss N, Mäkelä JP, McEvoy L, Hari R. Temporal integration and oscillatory response of the human auditory cortex revealed by evoked magnetic fields to click trains. Hearing Res 1993;68:89–96.

Franowicz MN, Barth DS. Comparison of evoked potentials and high-frequency (gamma-band) oscillating potentials in rat auditory cortex. J Neurophyisol 1995;74:96–112.

Galaburda A, Sanides F. Cytoarchitectonic organization of the human auditory cortex. J Comp Neurol 1980;190:597–610.

Galambos R, Makeig S, Talmachoff J. A 40 Hz auditory potential recorded from the human scalp. Proc Natl Acad Sci USA 1981; 78:2643–2647.

Galambos R A. Comparison of certain gamma band (40 Hz) brain rhythms in cat and man. In: Bullock TH, Basar E, editors. Induced rhythms in the brain, Bosten: Birkhäuser, 1991. pp. 201–206.

Geisler CD, Frishkopf LS, Rosenblith WA. Extracranial responses to acoustic clicks in man. Science 1958;128:1210–1211.

Grady CL, Van Meter J W, Maisog JM, Pietrini P, Krasuki J, Rauschecker JP. Attention-related modulation of activity in primary and secondary auditory cortex. NeuroReport 1997;8:2511–2516.

Hämäläinen MS, Sarvas J. Feasibility of the homogeneous head model in the interpretation of neuromagnetic fields. Phys Med Biol 1987;32:91–97.

Hari R, Hämäläinen M, Jousiniemi SL. Neuromagnetic steady-state responses to auditory stimuli. J Acoust Soc Am 1989;86:1033–1039.

Huotilainen M, Winkler I, Alho K, Escera C, Virtanen J, Ilmoniemi RJ, Jääkeläinen IP, Pekkonen E, Näätänen R. Combined mapping of human auditory EEG and MEG responses. Electroenceph clin Neurophysiol 1998;108:370–379.

Kosaki H, Hashikawa JH, Jones EG. Tonotopic organization of auditory cortical fields delineated by parvalbumin immunoreactivity in macaque monkeys. J Comp Neurol 1997;386:304–316.

Kraus N, Özdamar Ö, Hier D, Stein L. Auditory middle latency rsponses (MLRs) in patients with cortical lesions. Electroenceph clin Neurophysiol 1982;54:275–287.

Lee YS, Lueders H, Dinner DS, Lesser RP, Hahn J, Klem G. Recording of auditory evoked potentials in man using chronic subdural electrodes. Brain 1984;107:115–131.

Liegeois-Chauvel C, Musolino A, Chauvel P. Localization of the primary auditory area in man. Brain 1991;114:139–153.

Liegeois-Chauvel C, Musolino A, Badier JM, Marquis P, Chauvel P. Evoked potentials recorded from the auditory cortex in man: evaluation and topography of the middle latency components. Electroenceph clin Neurophysiol 1994;92:204–214.

Llinas RR, Ribary U. Rostrocaudal scan in human brain: A global characteristic of the 40-Hz response during sensory input. In: Bullock TH, Basar E, editors. Induced rhythms in the brain, Boston: Birkhäuser, 1991. pp. 147–154.

Makeig S. A dramatic increase in the auditory middle latency response at very slow rates. In: Brunia C, Gaillard A, Kok A, editors. Psychophysiological brain research, 2. Tilburg: Tilburg Univ. Press, 1990. pp. 60–64.

Mäkelä JP, Hari R. Evidence for cortical origin of the 40 Hz auditory evoked response in man. Electroenceph clin Neurophysiol 1987;66: 539–546.

Mäkelä JP, Hämäläinen MS, Hari R, McEvoy L. Whole-head mapping of middle-latency auditory evoked magnetic fields. Electroenceph clin Neurophysiol 1994;92:414–421.

Morel A, Kaas JH. Subdivisions and connections of auditory cortex in owl monkeys. J Comp Neurol 1992;318:27–63.

Morel A, Garraghty PE, Kaas JH. Tonotopic organization, architectonic fields and connections of auditory cortex in macaque monkeys. J Comp Neurol 1993;335:437–459.

Olshausen BA, Anderson CH, Van Essen DC. A neurobiological model of visual attention and invariant pattern recognition based on dynamic routing of information. J Neurosci 1993;13:4700–4719.

Özdamar Ö, Kraus N, Curry F. Auditory brain stem and middle latency response in a patient with cortical deafness. Electroenceph clin Neurophysiol 1982;53:224–230.

Özdamar Ö, Kraus N. Auditory middle-latency responses in humans. Audiology 1983;22:34–49.

Pantev C, Makeig S, Hoke M, Galambos R, Hampson S, Gallen C. Human auditory evoked gamma-band magnetic fields. Proc Natl Acad Sci USA 1991;88:8996–9000.

Pantev C, Elbert S, Makeig S, Hampson S, Eulitz C, Hoke M. Relationship of transient and steady-state auditory evoked fields. Electroenceph clin Neurophysiol 1993;88:389–396.

Pantev C, Bertrand O, Eulitz C, Verkindt C, Hampson S, Schuierer G, Elbert T. Specific tonotopic organizations of different areas of the human auditory cortex revealed by simultaneous magnetic and electric recordings. Electroenceph clin Neurophysiol 1995;94:26–40.

Pantev C, Roberts LE, Elbert T, Roβ B, Wienbruch C. Tonotopic organization of the sources of human auditory steady-state responses. Hearing Res 1996;101:62–74.

Pelizzone M, Hari R, Mäkelä JP, Huttunen J, Ahlfors S, Hämäläinen MS. Cortical origin of middle-latency auditory evoked responses in man. Neurosci Lett 1987;82:303–307.

Picton TW, Hillyard SA, Krausz HI, Galambos R. Human auditory evoked potentials. I: evaluation of components. Electroenceph clin Neurophysiol 1974;36:179–190.

Picton TW. Human auditory steady state responses. In: Barber C, Blum T, editors. Evoked potentials III, London: Butterworth, 1987. pp. 117–124.

Picton TW, Champagne SC, Kellett AJC. Human auditory evoked potentials recorded using maximum length sequences. Electroenceph clin Neurophysiol 1992;84:90–100.

Plourde G, Stapells DR, Picton TW. The human auditory steady-state evoked potentials. Acta Otolaryngol Suppl 1991;491:153–160.

Press WH, Teukolsky SA, Vetterling WT, Flannery BP. Numerical recipes. Cambridge: Cambridge University Press, 1992.

Rauschecker JP, Tian B, Hauser M. Processing of complex sounds in the macaque nonprimary auditory cortex. Science 1995;268:111–114.

Rauschecker JP, Tian B, Pons T, Mishkin M. Serial and parallel processing in rhesus monkey auditory cortex. J Comp Neurol 1997; 382:89–103.

Regan D. Some characteristics of average steady-state and transient responses evoked by modulated light. Electroenceph clin Neurophysiol 1965;20:238–248.

Regan D. Comparison of transient and steady-state methods. Ann NY Acad Sci 1982;388:45–71.

Ribary U, Ioannides AA, Singh KD, Hasson R, Bolton JPR, Lado F, Mogilner A, Llinas R. Magnetic field tomography of coherent thalamocortical 40-Hz oscillations in humans. Proc Natl Acad Sci USA 1991;88:11037–11041.

Romani GL, Williamson SJ, Kaufman L. Tonotopic organization of the human auditory cortex. Science 1982;216:1339–1340.

Santarelli R, Maurizi M, Conti G, Ottaviani F, Paludetti G, Pettorossi VE. Generation of human auditory steady-state responses (SSRs). II. Addition of responses to individual stimuli. Hearing Res 1995;83:9–18.

Scherg M, Volk SA. Frequency specificity of simultaneously recorded early and middle latency auditory evoked potentials. Electroenceph clin Neurophysiol 1983;56:443–452.

Scherg M, von Cramon D. Two bilateral sources of the late AEP as identified by a spatio-temporal dipole model. Electroenceph clin Neurophysiol 1985;62:32–44.

Scherg M, von Cramon D. Evoked dipole source potentials of the human auditory cortex. Electroenceph clin Neurophysiol 1986;65:344–360.

Scherg M, Hari R, Hämäläinen M. Frequency-specific sources of the auditory N19–P30–P50 response detected by a multiple source analysis of evoked magnetic fields and potentials. In: Williamson SJ, Hoke M, Sroink G, Kotani M, editors. Advances in biomagnetism, New York: Plenum Press, 1989a. pp. 97–100.

Scherg M, Vajsar J, Picton TW. A source analysis of the human auditory evoked potentials. J Cogn Neurosci 1989b;1:336–354.

Scherg M. Fundamentals of dipole source analysis. In: Grandori F, Hoke M, Romani GL, editors. Adv Audiol, vol 6.: Auditory evoked magnetic fields and electric potentials, Basel: Karger, 1990. pp. 40–69.

Scherg M, von Cramon D. Dipole source potentials of the auditory cortex in normal subjects and in patients with temporal lobe lesions. In: Grandori F, Hoke M, Romani GL, editors. Adv Audiol, vol 6.: Auditory evoked magnetic fields and electric potentials, Basel: Karger, 1990. pp. 165–193.

Stapells DR, Galambos R, Costello JA, Makeig S. Inconsistency of auditory middle latency and steady-state responses in infants. Electroenceph clin Neurophysiol 1988;71:289–295.

Vaughan Jr HG, Ritter W. The sources of auditory evoked responses recorded from the human scalp. Electroenceph clin Neurophysiol 1970;28:360–367.

Woldorff MG, Hillyard SA. Modulation of early auditory processing during selective listening to rapidly presented tones. Electroenceph clin Neurophysiol 1991;79:170–191.

Woldorff MG. Distortion of ERP averages due to overlap from temporally adjacent ERPs: Analysis and correction. Psychophysiology 1993;30:98–119.

Wood CC, Wolpaw JR. Scalp distribution of human auditory evoked potentials. II. evidence for overlapping sources and involvment of auditory cortex . Electroenceph clin Neurophysiol 1982;54:25–38.

Woods DL, Clayworth CC, Knight RT, Simpson GV, Naeser MA. Generators of middle- and long-latency auditory evoked potentials: implications from studies of patients with bitemporal lesions. Electroenceph clin Neurophysiol 1987;68:132–148.

Yoshiura T, Ueno S, Iramina K, Masuda K. Human middle latency auditory evoked magnetic fields. Brain Topogr 1996;8:291–296.